Available online at www.sciencedirect.com

ScienceDirect

Journal of Magnesium and Alloys 2 (2014) 27–35
www.elsevier.com/journals/journal-of-magnesium-and-alloys/2213-9567

Full length article

Effects of Mn addition on the microstructure and mechanical properties of cast Mg–9Al–2Sn (wt.%) alloy

Tianyu Zhu, Penghuai Fu*, Liming Peng, Xiaoyu Hu, Shouru Zhu, Wenjiang Ding

National Engineering Research Center of Light Alloy Net Forming and State Key Laboratory of Metal Matrix Composite, Shanghai Jiao Tong University, Shanghai 200240, PR China

Received 8 December 2013; revised 15 January 2014; accepted 17 January 2014
Available online 18 March 2014

Abstract

The microstructure and mechanical properties of cast Mg–9Al–2Sn–*x*Mn ($x = 0$, 0.1, 0.3 wt.%) alloys in as-cast, solution treated and aged conditions are investigated. The results reveal that Mn addition into Mg–9Al–2Sn alloy leads to the formation of $Al_8(Mn,Fe)_5$ phases, the grain refinement and the increase of discontinuous $Mg_{17}Al_{12}$ precipitates along the grain boundaries. 0.1 wt.% Mn addition has an obvious effect on accelerating the aging behavior of Mg–9Al–2Sn alloy at the early aging period up to 8 h, while 0.3 wt.% Mn addition alloy has an comparable aging behavior with the Mn-free alloy. Mn addition has less influence on the fracture behavior of Mg–9Al–2Sn alloy, while the fracture pattern is mainly determined by the thermal conditions. Mg–9Al–2Sn–0.1Mn alloy has the best combination of strength and elongation when aged at 200 °C for 8 h and the yield strength, ultimate tensile strength and elongation are 154 MPa, 292MPa and 5%, respectively.

Keywords: Mg–9Al–2Sn; Mn; Grain refinement; Precipitate; Cleavage plane

1. Introduction

Magnesium alloys are considered as promising materials in various fields such as automobiles, electronic production and aerospace due to their extraordinary characteristics and lightweight to reduce the petrol consumption [1,2]. Mg–Al based alloys are the most widely applied commercial magnesium alloys, in which Al addition can improve the castability and mechanical properties at room temperature. However, the discontinuous precipitates – $Mg_{17}Al_{12}$ inter-metallic along the boundary are reasonable to decrease the creep resistance at elevated temperature (120–150 °C), which limits the application of Mg–Al based alloys. Thus, researches tried to improve the creep resistance by adding some other elements to form some sorts of thermal stable precipitates or decrease the discontinuous $Mg_{17}Al_{12}$ phases along the grain boundaries. For instance, some rare earth (RE) elements, such as Ce, Nd, Y and Pr, can improve the creep resistance of Mg–Al based alloys by forming Al_3RE and $Al_{11}RE_3$ phases [3,4]. However, the application of the Mg–Al–RE alloys is limited due to the high cost of rare earth and some policies. Therefore, Mg–Al based alloy should be modified by inexpensive elements based on the consideration of their further application, such as Mg–Al–Ca alloy [5], Mg–Al–Sn-(Ca, Sr) alloy [6,7]. Recently, Mg–Sn system was well studied as the age-hardening alloy system due to the precipitation of Mg_2Sn phases (fcc structure), which is stable at high temperature (melting point is about 1043 K (770 °C)) [8,9]. Our previous investigation [7] indicated that, compared with commercial cast AZ91 alloy, some of cast

* Corresponding author. Tel.: +86 21 54742911; fax: +86 21 34202794.
E-mail address: fph112sjtu@sjtu.edu.cn (P. Fu).
Peer review under responsibility of National Engineering Research Center for Magnesium Alloys of China, Chongqing University.

Production and hosting by Elsevier

http://dx.doi.org/10.1016/j.jma.2014.01.003.

Mg–Al–Sn alloys have better tensile properties, especially Mg–9Al–2Sn (AT92) (wt.%) alloys. Mn addition can sharply enhance the corrosion resistance of AT92 alloy, which was proved to be useful in commercial alloys, such as AZ91D and AZ31 alloys [10,11]. However, the influences of Mn addition on the mechanical properties of AT92 alloy are still unclear. It was reported that Mn addition can refine the grains in Mg–Al based alloys in the form of Al_8Mn_5/$Al_8(Mn,Fe)_5$ phases [12,13]. While some researchers [14] stated that Al_8Mn_5 compounds were not sufficient nucleate sites because of the atomic row matching cross the interface between the matrix and the compounds. In addition, Y. Tamura et al. [15] found that the continuous precipitates preferentially occurred in the regions rich in Mn element during aging treatment. Based on the above review, Mn addition could modify the microstructure of Mg–Al based alloys. However, the influences of Mn addition on mechanical properties were not systematically studied yet. Therefore, in the present study, the influences of Mn addition on the microstructure and mechanical properties of cast Mg–9Al–2Sn (wt.%) alloy were studied at ambient temperature.

2. Experimental procedure

2.1. Materials and casting

Three kinds of Mg–9Al–2Sn–xMn (x = 0, 0.1, 0.3 wt.%, hereafter all compositions are in wt.% except otherwise stated) alloys were prepared from high purity magnesium, aluminum, tin ingots and Al–10Mn master alloy in a mild steel crucible with an electrical resistance furnace under the protection of a mixed gas of SF_6, CO_2 and dry air. They were heated to 740 °C ± 10 °C and gravity cast into a permanent mold after being held isothermally for 30 min. The mold was preheated at 400 °C and those ingots and master alloys were preheated at 200 °C. The actual chemical analysis of investigated alloys analyzed by spark spectrum was given with the average value in Table 1. After being cast, the specimens were solution treated at 420 °C for 16 h (T4) followed by water quenching at 25 °C and then isothermal aging treated at 200 °C from 0.5 h to 256 h (T6), respectively. Then specimens were cut from the ingots for tensile testing and microstructure observation at room temperature.

2.2. Microstructure analyzing and mechanical testing

Polished specimens for microstructure analysis were etched in 4 vol.% natal. The microstructure was examined with an optical microscopy (OM) and JEOL JSM-6460 scanning electron microscope (SEM) with an attached energy dispersive spectroscope (EDS). Vickers hardness was measured on a Semi-Vickers Hardness Tester using 5 kg load applied and at least 15 indentations were tested for each specimen. Flat tensile samples with dimensions of 3.5 mm in width, 2 mm in thick and 10 mm in length were cut from the plate castings and tested on the mechanical properties at room temperature on a Zwick/Roell 20 kN material test machine at a crosshead speed of 1 mm/min. Three tensile samples were tested for each thermal condition. Fracture surfaces of the tensile test samples were investigated by SEM and the microstructure near the fracture surface was observed by OM. The area fraction of both the secondary phases and the discontinuous precipitates were measured from the optical micrographs after isothermal aging treatment and the average grain size was also measured from the optical micrographs based on at least three images using the linear intercept method.

Table 1
Chemical composition of cast Mg–9Al–2Sn–xMn alloys, unit (wt.%).

	Al	Sn	Mn	Cu	Si	Fe	Mg
Mg–9Al–2Sn	8.44	1.79	0.01	0.006	0.07	0.0045	Bal.
Mg–9Al–2Sn–0.1Mn	8.52	1.74	0.11	0.004	0.05	0.0056	Bal.
Mg–9Al–2Sn–0.3Mn	8.31	1.61	0.34	0.010	0.09	0.0075	Bal.

3. Results

3.1. Microstructure

Fig. 1 presents the as-cast and solution-treated microstructure of cast Mg–9Al–2Sn-xMn (wt.%) (x = 0, 0.1, 0.3) alloys. All three as-cast alloys show the dendrites of α-Mg matrix surrounded by divorced eutectic compounds, as shown in Fig. 1a, c and e. Our previous study [7] confirmed that Mg–9Al–2Sn (AT92) alloy consists of α-Mg, $Mg_{17}Al_{12}$ and Mg_2Sn phases in the as-cast microstructure. Therefore, in Fig. 1a, the bright compounds are $Mg_{17}Al_{12}$ phases, while the black phases are Mg_2Sn phases. Besides, some eutectics of the mixture of α-Mg and discontinuous $Mg_{17}Al_{12}$ phases can also be observed (indicated in Fig. 1). When Mn element is added into AT92 alloy, besides the similar phases as AT92 alloy (Fig. 1a), some Mn-bearing particles, also in black color, can be investigated in AT92–0.1Mn (Fig. 1c) and AT92–0.3Mn (Fig. 1e) alloys. After solution treatment, the eutectics, $Mg_{17}Al_{12}$ and Mg_2Sn phases are almost all dissolved into the matrix (Fig. 1b, d and f) and a homogenized solid solution is formed. There are also some black particles at grain interiors in AT92 alloy (Fig. 1b), which should be the C-bearing particles related to the native grain refinement according the previous study [16]. Some residual Mg_2Sn phases can also be observed near the grain boundaries, which can be clearly observed on the fracture surface later. In AT92–0.1Mn and AT92–0.3Mn alloys, besides the residual Mg_2Sn phases, Mn-bearing particles can be found at the grain interiors. The Mn-bearing particles in AT92–0.3Mn alloy are larger (in the range of 4.69–7.81 μm in size) than those in AT92–0.1Mn alloy (~3.13 μm).

The average grain size measured by the linear intercept method in OM images are listed in Table 2. The addition of 0.1Mn and 0.3Mn can obviously refine the grain size from 154 μm of AT92 alloy to 114 μm of AT92–0.1Mn alloy and 110 μm of AT92–0.3Mn alloy in solution treated condition. Meanwhile, this refinement effects are also observed in different aging conditions (Table 2) when aging time varies from 0.5 h up to 4 h. However, there is little difference of the

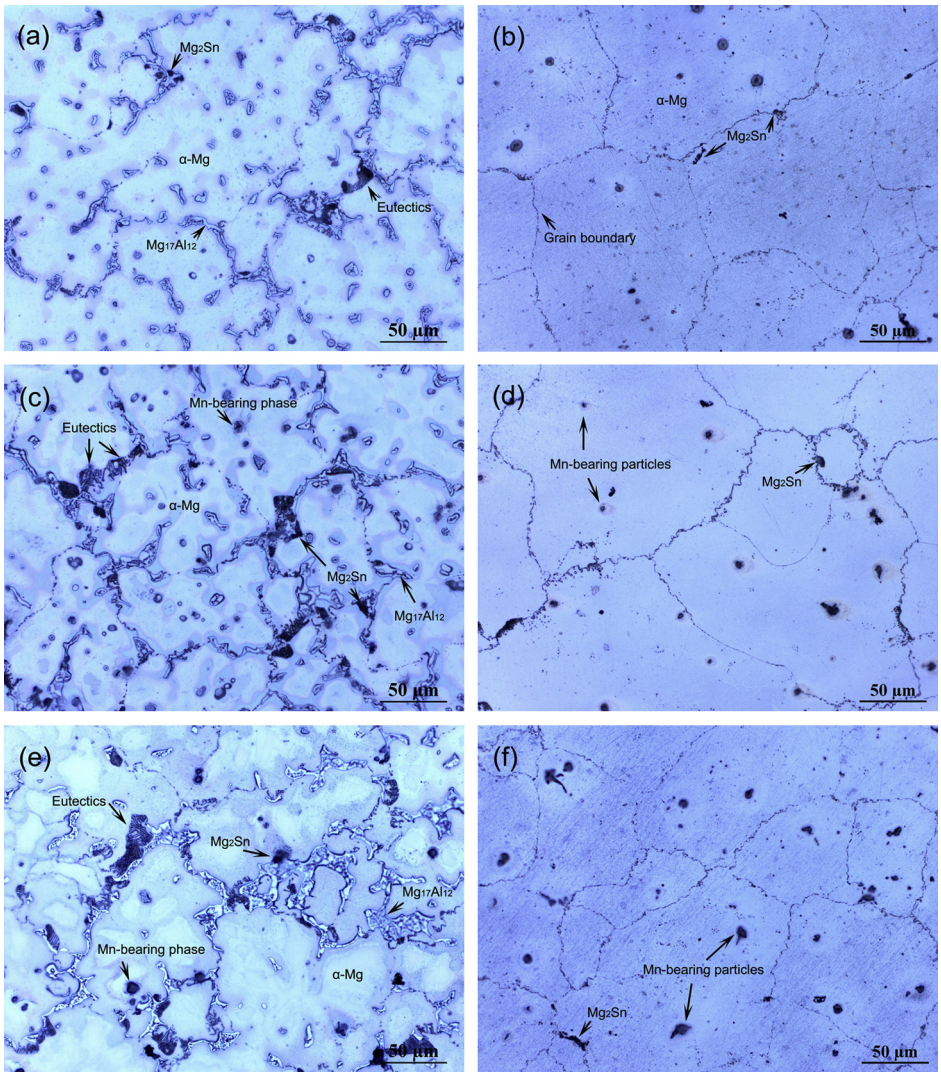

Fig. 1. Optical microstructure of as-cast and solution-treated Mg−9Al−2Sn−xMn (wt.%) alloys: (a) $x = 0$, as-cast alloy; (b) $x = 0$, solution-treated alloy; (c) $x = 0.1$, as-cast alloy; (d) $x = 0.1$, solution-treated alloy; (e) $x = 0.3$, as-cast; (f) $x = 0.3$, solution-treated alloy.

grain refinement effect between 0.1Mn and 0.3Mn addition alloys.

Fig. 2 presents the OM images of 200 °C aging treated Mg−9Al−2Sn−xMn alloys ($x = 0$, 0.1, 0.3) at different aging times (t) from 0.5 h up to 4 h. Subsequent aging treatment after solution treatment leads to two different kinds of $Mg_{17}Al_{12}$ precipitates, which are already confirmed by the previous studies [17,18] − discontinuous and continuous $Mg_{17}Al_{12}$ precipitates. The present study examines the variation of the volume percentage of discontinuous $Mg_{17}Al_{12}$ precipitates with the aging time variation from 0.5 h to 4 h, since it is difficult to distinguish the discontinuous precipitates from the continuous precipitates when aging time is longer than 4 h. At the beginning of aging, the discontinuous precipitates lead to the shadows in OM images, therefore, it is easy to distinguish the discontinuous precipitates from the matrix. These shadows, of course, do not merely consist of all of the discontinuous precipitates, but are the mixture of discontinuous $Mg_{17}Al_{12}$ phases and α-Mg. In present study, the area percentage of the shadows was used to represent the content of the discontinuous

Table 2
Average grain size of cast Mg−9Al−2Sn−xMn alloys measured by the linear intercept method in OM images, unit (μm).

	Mg−9Al−2Sn	Mg−9Al−2Sn−0.1Mn	Mg−9Al−2Sn−0.3Mn
Solution-treated	153.9 ± 11.3	113.9 ± 4.0	110.1 ± 9.5
420 °C × 16 h + 200 °C × 0.5 h	105.8 ± 3.0	94.2 ± 10.4	102.5 ± 4.5
420 °C × 16 h + 200 °C × 1 h	103.2 ± 2.1	82.6 ± 4.4	87.9 ± 12.7
420 °C × 16 h + 200 °C × 2 h	125.5 ± 16.6	97.9 ± 5.3	96.0 ± 8.3
420 °C × 16 h + 200 °C × 4 h	137.0 ± 1.9	113.8 ± 5.1	130.5 ± 8.3

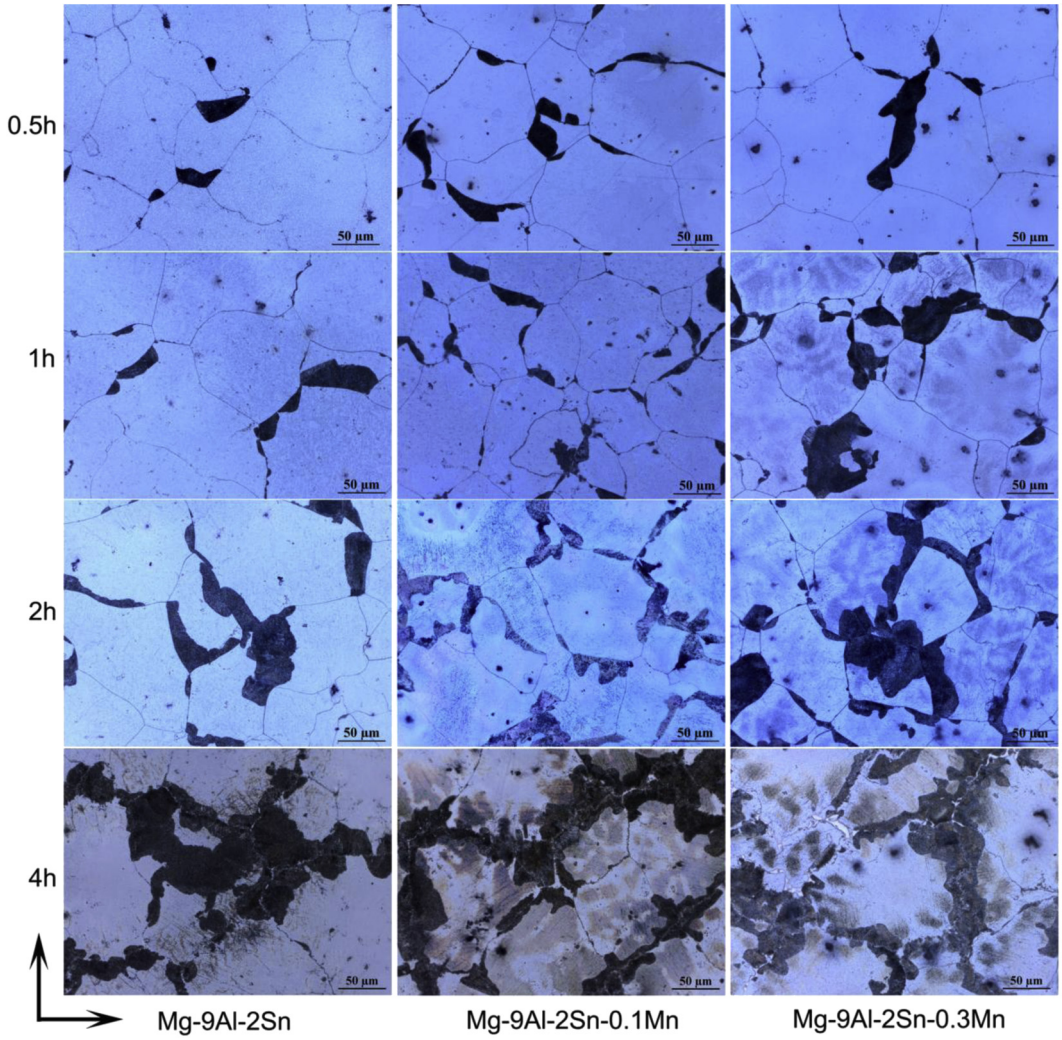

Fig. 2. Optical microstructure of aging treated Mg−9Al−2Sn−xMn alloys (x = 0, 0.1, 0.3 wt.%) at different aging times (t) from 0.5 h up to 4 h.

precipitates and the results are list in Table 3. It indicates that the discontinuous precipitates increase when Mn element is added. Mn addition seems to accelerate the precipitation of discontinuous $Mg_{17}Al_{12}$ phases. Such effect is much clearer at shorter aging times, such as 0.5 h, 1 h and 2 h.

Fig. 3 shows the SEM images of cast AT92−0.3Mn alloy aged at 200 °C for 64 h. The discontinuous precipitates were observed along the grain boundary, whose size is obviously larger than the continuous precipitates at grain interiors, as indicated by the arrows in Fig. 3a. The chemical concentrations of the phases with different contrasts were measured by EDS and the results are listed in Table 4. The large white protrusions (spectrums 1 and 2) are supposed to be Al_8(Mn, Fe)$_5$ particles based on their chemical composition and the previous study [14], which can also be observed in OM images of Fig. 1d and f in gray color. The fine white particles (spectrum 3 in Fig. 3b) along with the discontinuous precipitates (spectrum 4) and the residual $Mg_{17}Al_{12}$ phases are Mg_2Sn phases according to their chemical compositions.

3.2. Aging curves

Fig. 4 demonstrates the aging behavior of the investigated alloys with and without Mn addition isothermal aging treated at 200 °C. The aging curves of AT92, AT92−0.1Mn and AT92−0.3Mn alloys look similar to each other. The hardness

Table 3
Ratios of shadow area of cast Mg−9Al−2Sn−xMn (wt.%) alloys aged at 200 °C from 0.5 h to 4 h, unit (%).

	Mg−9Al−2Sn	Mg−9Al−2Sn-0.1Mn	Mg−9Al−2Sn−0.3Mn
420 °C × 16 h + 200 °C × 0.5 h	1.12 ± 0.37	1.65 ± 0.08	2.86 ± 0.21
420 °C × 16 h + 200 °C × 1 h	6.73 ± 0.70	7.74 ± 0.58	7.34 ± 0.18
420 °C × 16 h + 200 °C × 2 h	10.48 ± 0.56	12.15 ± 1.28	13.75 ± 0.54
420 °C × 16 h + 200 °C × 4 h	29.89 ± 0.92	33.65 ± 0.34	29.79 ± 0.36

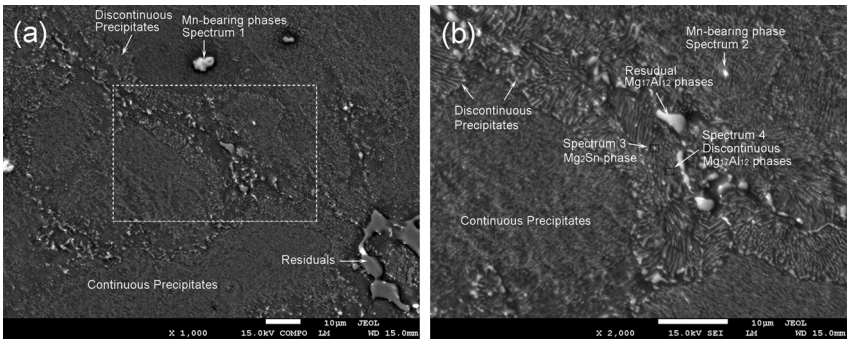

Fig. 3. SEM micrographs of cast Mg−9Al−2Sn−0.3Mn alloy aged at 200 °C for 64 h after solution treatment. Image (b) is the high-magnification observation of area indicated by the square in image (a).

Table 4
Chemical concentration of investigated area (spectrum 1, 2, 3, 4) in Fig. 5 with EDS analysis.

Element	Spectrum 1		Spectrum 2		Spectrum 3		Spectrum 4	
	Weight%	Atomic%	Weight%	Atomic%	Weight%	Atomic%	Weight%	Atomic%
MgK	24.20	33.88	59.14	65.38	81.01	87.01	84.75	87.45
AlK	37.53	47.34	29.79	29.68	11.79	11.40	12.96	12.06
MnK	22.73	14.08	8.66	4.24	–	–	0.05	0.02
FeL	0.74	0.45	0.61	0.29	–	–	–	–
SnL	14.80	4.25	1.80	0.41	7.20	1.58	2.23	0.47

of all of three alloys drops from as-cast condition to solution treated condition, keeps increasing from 0 h (solution treated condition) up to 64 h and decreases after that. The hardness decrease of Mg−9Al−2Sn−xMn alloys after solution treatment is due to the dissolution of $Mg_{17}Al_{12}$ and Mg_2Sn phases. Their difference of aging curves mainly locates at the early period of aging process from 0.5 h to 64 h. The hardness of AT92−0.1Mn alloy (red line in Fig. 4) increases much more rapidly than the other two alloys, as seen from the slopes of the aging curves from 0.5 h to 8 h in Fig. 4. At the peak-aged condition, the hardness increase (ΔHV) of the investigated alloys are 28HV (0Mn), 33HV (0.1Mn), 30HV (0.3Mn), respectively. AT92−0.1Mn alloy has the highest hardness

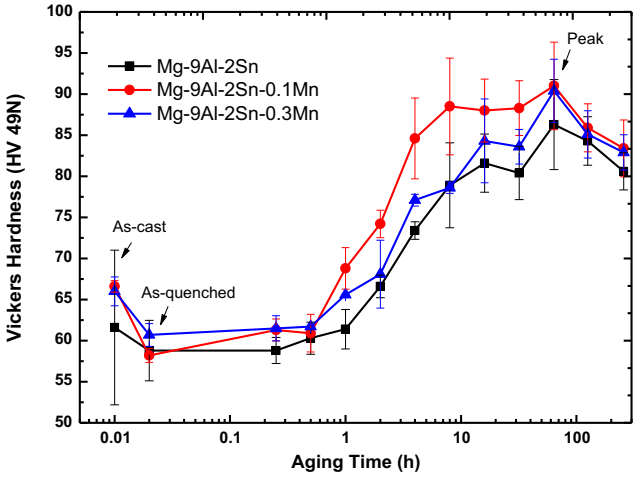

Fig. 4. Vickers hardness evolution of cast Mg−9Al−2Sn−xMn (wt.%) alloys under isothermal aging condition at 200 °C.

increment (For interpretation of the references to color in this paragraph, the reader is referred to the web version of this article.).

3.3. Tensile properties

Tables 5–7 list the yield strength, ultimate tensile strength and elongation of cast Mg−9Al−2Sn−xMn (x = 0, 0.1, 0.3) alloys in different thermal treated conditions at room temperature. Table 5 demonstrates that the yield strength decreases from as-cast condition to solution treated condition and increases with aging time, gets its peak at 8 h and decreases after that. The peak yield strength of three alloys are 133 MPa (0Mn), 154 MPa (0.1Mn) and 137 MPa (0.3Mn) respectively, where AT92−0.1Mn alloy has the highest yield strength of 154 MPa. The variation of elongation is nearly in an opposite way (Table 7). The elongation decreases with the increase of aging time. Generally, the Mn containing alloys (AT92−0.1Mn and AT92−0.3Mn) have a little bit better elongation than the Mn-free alloy (AT92). The variation of ultimate tensile strength is generally irregular and the Mn containing alloys have higher ultimate tensile strength than the Mn-free alloy (Table 6). AT92−0.1Mn alloy has the best combination of yield strength, ultimate tensile strength and elongation when aged at 200 °C for 8 h, which are 154 MPa, 292MPa and 5%, respectively.

3.4. Fracture surface

Fig. 5 depicts the SEM images of the fracture surface of the studied alloys tensile tested at as-cast, solution treated and T6 (200 °C × 8 h) conditions. The failure surfaces of as-cast

Table 5
Yield strength of cast Mg–9Al–2Sn–xMn (x = 0, 0.1, 0.3 wt.%) alloys at different aging treatments: as-cast, T4 and T6 condition, unit (MPa).

Thermal conditions	Mg–9Al–2Sn	Mg–9Al–2Sn-0.1Mn	Mg–9Al–2Sn-0.3Mn
As-cast	94.52 ± 0.60	105.19 ± 1.76	112.21 ± 5.00
Solution-treated	90.49 ± 0.94	95.35 ± 3.79	97.30 ± 1.73
420 °C × 16 h + 200 °C × 0.5 h	91.02 ± 0.42	99.77 ± 2.77	105.00 ± 1.38
420 °C × 16 h + 200 °C × 1 h	97.28 ± 0.96	109.10 ± 2.67	105.60 ± 1.73
420 °C × 16 h + 200 °C × 2 h	119.06 ± 3.73	125.75 ± 9.44	119.73 ± 6.80
420 °C × 16 h + 200 °C × 4 h	128.02 ± 5.48	142.13 ± 6.21	125.89 ± 3.51
420 °C × 16 h + 200 °C × 8 h	133.71 ± 27.8	154.44 ± 2.63	137.42 ± 11.2
420 °C × 16 h + 200 °C × 64 h	120.45 ± 7.15	138.81 ± 2.16	133.66 ± 4.53

alloys consist of fractured eutectics or secondary compounds, as shown in Fig. 5a, d and g. As the atomic number of Mg and Al elements is very close, in backscattered electron images, only the fractured Mg_2Sn compounds can be clearly distinguished, which can be seen in the inset images at the corners of Fig. 5a, d and their locations are indicated by rectangles. Also, lots of secondary cracks (arrows) can be observed, which reveals that these alloys are brittle in general. Different from as-cast alloys, there are lots of fractured cleavage planes on the fracture surfaces of solution treated (Fig. 5b, e and h) and aged (Fig. 5c, f and i) alloys. Some of the cleavage planes are grain-size large, and probably the whole grains fracture along the cleavage planes. Beside the cleavage planes, there are fine dimples on these fracture surfaces. Amplified images can be found in Fig. 6. These dimples are probably located near grain boundaries as lots of residuals (Mg_2Sn compounds) can be observed. There are also fine residuals (fine white particles in Fig. 6b) among the dimples. However, these fine residuals should not be the reasons to form the dimples, because lots of dimples are not related to the fine residuals as indicated by the arrow in Fig. 6. These dimples should be formed by the activation of non-basal slips near the grain boundaries where experience severe plastic deformation during the fracture. Therefore, the as-cast alloys mainly failure through the eutectics or secondary compounds, which is inter-granular fracture pattern, and solution treated and aged alloys fracture in a mixture pattern of trans-granular and inter-granular, where trans-granular pattern is dominant. There is no obvious difference among the three alloys.

Fig. 7 shows the optical microstructure of ruptured samples perpendicular to the fracture surface of cast Mg–9Al–2Sn–xMn (x = 0, 0.1, 0.3) alloys in T6 − 4 h condition. The discontinuous precipitates − $Mg_{17}Al_{12}$ phases (dark shadows) are locates along the grain boundaries. Cracks near the fracture surface are observed, which mainly locate at the inside of grains. Some of the cracks are generated along the basal slip planes as parallel slip lines can be observed, as indicated in Fig. 7a. While some of the cracks present certain angles with the parallel slip lines, as indicated in Fig. 7a and c, which may be fracture along the twinning boundaries, or just along the twinning boundaries, as shown in Fig. 7b. Therefore, the cleavage planes observed on the fracture surfaces in Fig. 5 are probably the basal planes or twinning boundaries. Coincident with the observation of fracture surface (Fig. 5), the OM observation also confirms that the alloys in aged condition fractures in a mixture mode of inter-granular and trans-granular patterns, as both fractured cleavage planes and grain boundaries can be observed (Fig. 7a, b).

4. Discussion

From the above description, Mn addition into cast Mg–9Al–2Sn (AT92) alloy has influences both on microstructure and mechanical properties.

When Mn is added into the alloy, $Al_8(Mn, Fe)_5$ particles form at the grain interiors (Fig. 1). The size of these particles grows with the increase of Mn addition. $Al_8(Mn, Fe)_5$ particles in AT92–0.3Mn alloy are in the range of 4.69–7.81 μm, larger than those in AT92–0.1Mn alloy (∼3.13 μm), as shown in Fig. 1d and f. The size of these $Al_8(Mn, Fe)_5$ particles seems not to change during solution treatment. For instance, the size of $Al_8(Mn, Fe)_5$ particles in solution treated AT92–0.1Mn alloy is still about 3 μm (Fig. 1d), nearly the same as that of as-cast alloy. Mn addition leads to the grain refinement of AT92 alloy, which is confirmed in both solution treated and different aged conditions in Table 2. Such phenomenon of

Table 6
Ultimate tensile strength of cast Mg–9Al–2Sn–xMn (x = 0, 0.1, 0.3 wt.%) alloys at different aging treatments: as-cast, T4 and T6 condition, unit (MPa).

Thermal conditions	Mg–9Al–2Sn	Mg–9Al–2Sn-0.1Mn	Mg–9Al–2Sn-0.3Mn
As-cast	204.07 ± 13.24	197.98 ± 14.26	210.91 ± 11.99
Solution-treated	276.02 ± 2.42	278.84 ± 6.71	256.25 ± 1.91
420 °C × 16 h + 200 °C × 0.5 h	247.82 ± 0.49	289.79 ± 7.58	291.86 ± 3.32
420 °C × 16 h + 200 °C × 1 h	262.96 ± 0.38	298.59 ± 10.93	305.86 ± 1.72
420 °C × 16 h + 200 °C × 2 h	267.56 ± 17.77	280.85 ± 24.91	268.56 ± 1.68
420 °C × 16 h + 200 °C × 4 h	273.52 ± 17.89	269.20 ± 8.45	259.89 ± 12.69
420 °C × 16 h + 200 °C × 8 h	250.33 ± 4.46	292.48 ± 3.32	271.59 ± 15.77
420 °C × 16 h + 200 °C × 64 h	237.41 ± 11.06	267.11 ± 0.78	237.52 ± 12.90

Table 7
Elongation of cast Mg–9Al–2Sn-xMn (x = 0, 0.1, 0.3 wt.%) alloys at different aging treatments: as-cast, T4 and T6 condition, unit (%).

Thermal conditions	Mg–9Al–2Sn	Mg–9Al–2Sn-0.1Mn	Mg–9Al–2Sn-0.3Mn
As-cast	5.64 ± 1.14	4.42 ± 1.55	5.41 ± 0.70
Solution-treated	12.39 ± 4.45	11.20 ± 0.93	9.53 ± 0.42
420 °C × 16 h + 200 °C × 0.5 h	10.81 ± 1.02	14.29 ± 0.4	13.81 ± 0.09
420 °C × 16 h + 200 °C × 1 h	9.02 ± 0.29	11.40 ± 1.5	12.78 ± 0.31
420 °C × 16 h + 200 °C × 2 h	7.12 ± 1.14	7.90 ± 2.06	7.68 ± 0.53
420 °C × 16 h + 200 °C × 4 h	5.82 ± 0.73	4.42 ± 0.76	6.29 ± 0.80
420 °C × 16 h + 200 °C × 8 h	2.45 ± 0.28	4.96 ± 0.68	4.67 ± 0.62
420 °C × 16 h + 200 °C × 64 h	3.51 ± 0.40	4.67 ± 0.01	3.11 ± 0.68

grain refinement probably causes by the formation of $Al_8(Mn, Fe)_5$ particles, since $Al_8(Mn, Fe)_5$ could be effective nuclei in Mg alloys [12,13]. Though there is still a debate on the grain refinement effect of $Al_8(Mn, Fe)_5$ particles, the present experiment supports the idea that $Al_8(Mn, Fe)_5$ particles have some effect of grain refinement. The addition of Mn element also seems to increase the content of discontinuous precipitates (the shadow area in Fig. 2) of AT92 alloy. Therefore, in a summary, the addition of Mn element into AT92 alloy leads to the formation of $Al_8(Mn, Fe)_5$ particles, certain grain refinement effect and the increase of the content of discontinuous precipitates.

The influences of Mn addition on the mechanical properties are mainly indicated by the change of aging curves (Fig. 4) and the improvement of yield strength (Table 5). It seems that 0.1Mn addition has much more obvious effect on the mechanical properties than 0.3Mn addition. The hardness of AT92–0.1Mn alloy increases much more rapidly than the other two alloys, and can be seen from the slopes of the aging curves from 0.5 h to 8 h in Fig. 4. It then leads to the highest yield strength of 154 MPa when aged at 200 °C for 8 h. It seems that 0.1Mn addition promotes the aging hardening ability of AT92 alloy. A recent research about Mg–2Al–2Ca alloy [19] shows that the average diameter of the GP zone

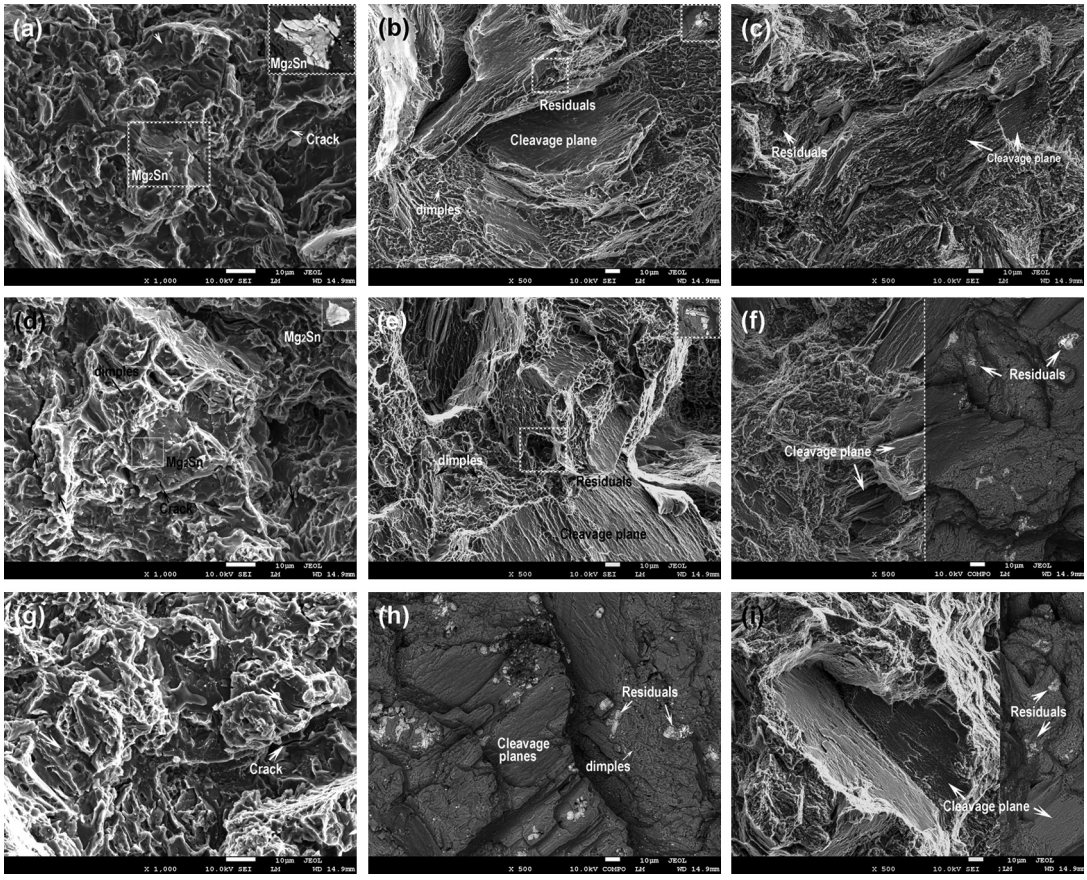

Fig. 5. SEM fractographs of cast Mg–9Al–2Sn–xMn (x = 0, 0.1, 0.3 wt.%): x = 0, (a) as-cast, (b) solution-treated, (c) aging treated – 8 h; x = 0.1, (d) as-cast, (e) solution-treated, (f) aging treated – 8 h; x = 0.3, (g) as-cast, (h) solution-treated, (i) aging treated – 8h. The insets are the backscatter images of the areas indicated by the rectangles in (a), (b), (d) and (e). The right parts of (f) and (i), the whole part of (h) are backscatter images.

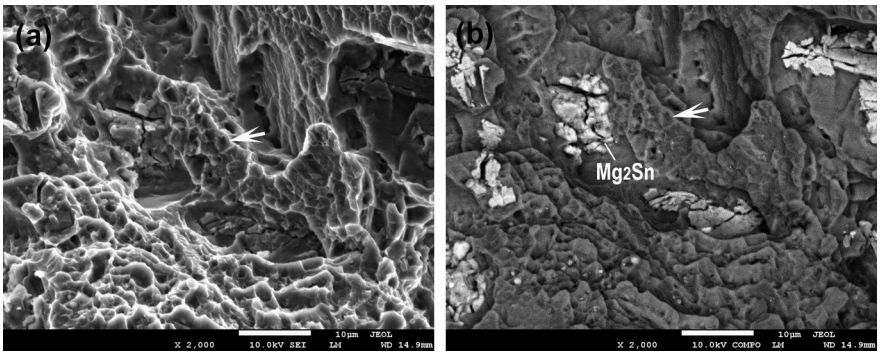

Fig. 6. SEM fractographs of solution treated Mg–9Al–2Sn–0.1Mn alloy: (a) secondary electron image, (b) backscatter electron image.

(Al–Ca) is decreased by Mn addition. Similar growth resistant effect of Mn addition on $Mg_{17}Al_{12}$ precipitates may also exist in present alloy, which may enhance the number density of continuous $Mg_{17}Al_{12}$ phases. Therefore, the improvement of mechanical properties of 0.1Mn addition alloy may be the results of the grain refinement effect of Mn addition (Table 2), the increase of discontinuous precipitates at grain boundaries and possible growth resistant effect of Mn addition on continuous precipitates at grain interiors.

Why 0.3Mn addition has less influence on both microstructure and mechanical properties than that of 0.1Mn addition? It is still unclear at present moment. However, similar results were observed in Peng Cao et al.'s research [13]. They reported that 0.1Mn addition can refine the grains of Mg–9Al alloy while 0.2Mn addition leads to a little bit coarser grains compared with Mg–9Al alloy. Therefore, it seems to be true in Mg–9Al based alloy that 0.1Mn addition has the best grain refinement effect. The behind reason should be revealed by further studies.

Another important issue needs to be revealed in present study is that the fractured residual Mg_2Sn compounds can be frequently observed on the fracture surfaces of AT92 series alloys, as shown in Fig. 5, even after solution treatment, such as Fig. 5e. These fractured Mg_2Sn compounds probably reduce the ductility of AT92 series alloys as they fracture into pieces easily. Therefore, Sn content in Mg–9Al–Sn alloy should decrease to ~1% for better mechanical properties, as the solution temperature (420 °C) in the present study is already very high for the Mg–9Al based alloy and cannot be enhanced any more.

5. Conclusion

The microstructure and mechanical properties of cast Mg–9Al–2Sn–xMn (x = 0, 0.1, 0.3 wt.%) alloys in as-cast, solution treated and aged conditions are investigated and the following conclusions can be drawn.

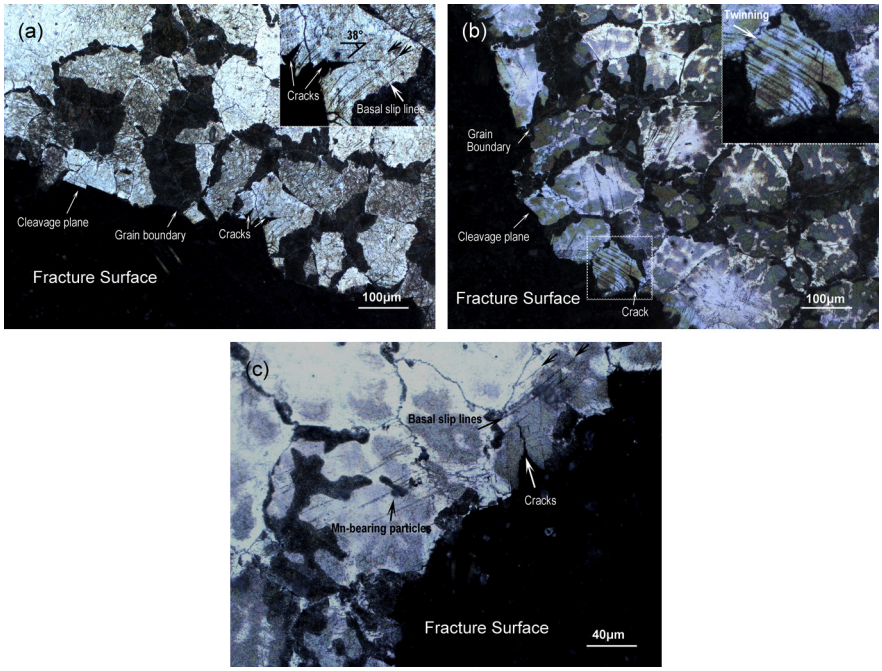

Fig. 7. Optical fracture of Mg–9Al–2Sn–xMn (x = 0, 0.1, 0.3 wt.%) with aging treatment at 200 °C for 4 h: (a) x = 0, (b) x = 0.1, (c) x = 0.3.

(1) Mn addition into Mg−9Al−2Sn alloy leads to the formation of $Al_8(Mn,Fe)_5$ phases, the grain refinement and the increase of discontinuous $Mg_{17}Al_{12}$ precipitates along the grain boundaries. The formation of $Al_8(Mn,Fe)_5$ particles at grain interiors are probably the reason of grain refinement, which are stable in size during the solution treatment.
(2) 0.1 wt.% Mn addition alloy has an obvious effect on accelerating the aging behavior of Mg−9Al−2Sn alloy at the early aging period up to 8 h and while 0.3 wt.% Mn addition alloy has an comparable aging behavior with the Mn-free alloy. Mg−9Al−2Sn−0.1Mn alloy has the best combination of strength and elongation when aged at 200 °C for 8 h and the yield strength, ultimate tensile strength and elongation are 154 MPa, 292MPa and 5%, respectively.
(3) Mn addition has less influence on the fracture behavior of Mg−9Al−2Sn alloy. The fracture patterns of cast Mg−9Al−2Sn−*x*Mn alloys are mainly determined by their thermal conditions. The as-cast alloys mainly fail through the eutectics or secondary compounds, which is inter-granular fracture pattern. The solution treated and aged alloys fracture in a mixture pattern of trans-granular and inter-granular, where trans-granular pattern is dominant. The cleavage planes observed on the fracture surfaces of solution treated and aged alloys are probably the basal planes or twinning boundaries.

Acknowledgment

This research work is collaborated by General Motors Global Research and Development (GM R&D), Warren, MI, USA, and Shanghai Jiao Tong University (SJTU), Shanghai, China. Dr P. Fu would like to acknowledge the support of a Specialized Research Fund for the Doctoral Program of Higher Education (20110073120008) and a project from Shanghai Science and Technology Committee (12DZ0501700).

References

[1] B.L. Mordike, T. Ebert, Mater. Sci. Eng., A 302 (2001) 37−45.
[2] Alan A. Luo, J. Magnesium Alloys 1 (2013) 2−22.
[3] Y. Lü, Q. Wang, X. Zeng, et al., Mater. Sci. Eng., A 278 (2000) 66−76.
[4] F. Khomamizadeh, B. Nami, S. Khoshkhooei, Metall. Mater. Trans. A 36 (2005) 3489−3494.
[5] Y. Lou, X. Bai, L. Li, Trans. Nonferrous Met. Soc. China 21 (2011) 1247−1252.
[6] B.H. Kim, K.C. Park, Y.H. Park, I.M. Park, Trans. Nonferrous Met. Soc. China 20 (2010) 1184−1191.
[7] A. Luo, P. Fu, L. Peng, et al., Metall. Mater. Trans. A 43 (2012) 360−368.
[8] C.L. Mendis, C.J. Bettles, M.A. Gibson, C.R. Hutchinson, Mater. Sci. Eng., A 435−436 (2006) 163−171.
[9] S. Wei, Y. Chen, Y. Tang, et al., Mater. Sci. Eng., A 492 (2008) 20−23.
[10] M. Jönsson, D. Thierry, N. LeBozec, Corros. Sci. 48 (2006) 1193−1208.
[11] R.C. Zeng, J. Zhang, W.J. Huang, et al., Trans. Nonferrous Met. Soc. China 16 (2006) s763−s771.
[12] S. Lun Sin, D. Dube, R. Tremblay, Mater. Charact. 58 (2007) 989−996.
[13] P. Cao, Q. Ma, D.H. StJohn, Scr. Mater. 54 (2006) 1853−1858.
[14] Y. Wang, M. Xia, Z. Fan, X. Zhou, G.E. Thompson, Intermetallics 18 (2010) 1683−1689.
[15] Y. Tamura, Y. Kida, H. Tamehiro, et al., J. Mater. Sci. 43 (2008) 1249−1258.
[16] P. Cao, Q. Ma, D.H. StJohn, Scr. Mater. 53 (2005) 841−844.
[17] K.N. Braszczyńska-Malik, J. Alloys Compd. 477 (2009) 870−876.
[18] M.-X. Zhang, P.M. Kelly, Scr. Mater. 48 (2003) 647−652.
[19] T. Hommaa, S. Nakawaki, K. Oh-ishi, K. Hono, S. Kamado, Acta Mater. 59 (2011) 7662−7672.